Nuclear Science and Techniques (2026) 37:41
https://doi.org/10.1007/s41365-025-01858-2

Bayesian neural network evaluation method on the neutron-induced fission product yields of ^{232}Th

Chun-Yuan Qiao[1] · Ya-Xuan Wang[1] · Chun-Wang Ma[1,2] · Jun-Chen Pei[3] · Yong-Jing Chen[4]

Received: 29 July 2025 / Revised: 9 November 2025 / Accepted: 24 November 2025 / Published online: 9 January 2026

Abstract
Research on neutron-induced fission product yields of ^{232}Th is crucial for understanding the competition between symmetric and asymmetric fission in actinide nuclei. However, obtaining complete isotopic yield distributions over a wide range of neutron energies remains a challenge. In this study, a Bayesian neural network model was developed to predict the independent (IND) and cumulative fission yields of ^{232}Th under neutron irradiation at various incident energies. To address the limited availability of experimental data for the analysis of IND mass distributions, we substituted mass-number-based yields with the yields of specific isotopes. Furthermore, physical phenomena or quantities, such as the odd–even effect and isospin, were introduced as constraints to enhance the physical consistency of the predictions. The impact of these constraints was evaluated using mass-chain yield distributions and their dependence on energy. Incorporating physical constraints significantly improves the prediction accuracy, yielding more reliable and physically meaningful fission yield data for nuclear physics and reactor design applications.

Keywords Bayesian neural network · ^{232}Th · Independent fission yield · Cumulative fission yield · Odd–even effect · Isospin

1 Introduction

Nuclear fission, a fundamental phenomenon in nuclear physics, plays a crucial role in a wide range of applications, including nuclear energy, national defense, and medical isotope production. It is also essential for studies on the synthesis of superheavy nuclei [1, 2], the analysis of reactor antineutrino energy spectra [3–5], and the investigation of nucleosynthesis via the r-process in neutron star mergers [6–8]. Accurate and comprehensive fission yield data are critical for understanding the dynamic evolution of fission process. In 2011, the Chinese Academy of Sciences launched the Strategic Priority Science and Technology Project entitled "Future Advanced Nuclear Fission Energy—Thorium Molten Salt Reactor (TMSR) Nuclear Energy System", employing ^{232}Th as the primary fuel [9]. The experimental TMSR reactor achieved its first criticality in October 2023. In this system, ^{232}Th serves as a key component, participating mainly in neutron-induced reactions via the Th-U fuel cycle [10]. In particular, high-energy neutrons may induce the direct fission of ^{232}Th. Consequently, for an accurate burn-up credit analysis, special attention must be paid to the fission product yields to reliably assess the reactivity feedback and characteristics of the spent fuel.

Currently, major international evaluated nuclear data libraries (such as JENDL [11], ENDF [12], CENDL [13], and JEFF [14]) provide comprehensive data for neutron-induced fission yields only at specific energies, that is, 0.0253 eV (thermal neutron), 0.5 MeV, and 14 MeV,

This work was supported by the National Natural Science Foundation of China (Nos. 12247126 and 12375123), Henan Postdoctoral Foundation (No. HN2024013), and the Natural Science Foundation of Henan Province (No. 242300421048).

✉ Chun-Wang Ma
machunwang@126.com

[1] School of Physics, Centre for Theoretical Physics, Henan Normal University, Xinxiang 453007, China

[2] Institute of Nuclear Science and Technology, Henan Academy of Sciences, Zhengzhou 450046, China

[3] State Key Laboratory of Nuclear Physics and Technology, School of Physics, Peking University, Beijing 100871, China

[4] China Nuclear Data Center, China Institute of Atomic Energy, Beijing 102413, China

respectively. However, the measured neutron-induced fission data are often sparse, with incomplete isotopic coverage, significant uncertainties, and notable discrepancies [15]. Obtaining complete isotopic yield distributions across a continuous range of incident neutron energies remains a challenge. Phenomenological models of nuclear fission (such as the Brosa [16] and GEF [17] approaches) rely heavily on experimental data for parameter calibration and validation. When such data are limited or absent, the underlying assumptions and approximations of these models become weakly constrained, resulting in increased parameter uncertainty and diminished predictive reliability. In the case of ^{232}Th, the lack of systematic fission yield measurements at various neutron energies further hampers the direct application of such semi-empirical models, highlighting the urgent need for alternative approaches to obtain complete yield data.

With the development of artificial intelligence, machine learning (ML) techniques have found extensive and diverse applications in nuclear physics research [18–20]. These applications encompass a wide range of studies, including the prediction of nuclear masses for advancing nuclear theory [21–24], astrophysical modeling [25–27], and methodological comparisons [28, 29]; the determination of nuclear charge radii [30–34]; the estimation of α-decay and β-decay half-lives [35–37]; the inference of ground-state spin parities [38]; and the prediction of fission product yields [39–43]. Furthermore, in the realm of nuclear reactions, ML has been effectively employed to model cross sections across various mechanisms, such as proton-induced spallation [44–47], projectile fragmentation [48–51], and photonuclear reactions [52, 53]. ML algorithms can uncover hidden patterns in complex datasets and extract the underlying physical correlations [54]. Among these approaches, the Bayesian neural network (BNN) has shown particularly strong potential for fission yield evaluation [39, 55]. The BNN rigorously quantifies uncertainties through the probabilistic treatment of model parameters [56], incorporates prior physical knowledge to enhance learning from limited datasets, and captures nonlinear features in yield distributions, such as the transition between asymmetric and symmetric fission modes [57–59]. Furthermore, its probabilistic framework ensures direct compatibility with modern nuclear data evaluation practices that require covariance data. The capability of BNN to integrate experimental uncertainties and missing data further enhances its robustness and predictive accuracy while mitigating overfitting [57–59]. This makes it a promising tool for reliable ^{232}Th fission yield predictions, where experimental data are sparse.

In this study, a Bayesian neural network (BNN) framework was employed to model and predict the fission product yields of ^{232}Th [39]. Guided by the findings of Ref. [60], the hyperbolic tangent (tanh) activation function was selected for its superior capability in capturing yield trends and reducing prediction errors. To balance the model complexity and accuracy, a two-hidden-layer architecture was adopted, which offers improved performance on complex fission datasets with a manageable number of trainable parameters. Therefore, a two-hidden-layer BNN architecture with tanh activation functions was adopted in this study. The network structure was further optimized by analyzing the error distributions to determine the appropriate number of neurons in each layer. In scenarios where experimental data are sparse, the inclusion of relevant physical constraints, such as the odd–even effect and isospin, has been shown to significantly enhance the predictive accuracy [61–64]. The BNN predictions incorporating the odd–even effect and isospin showed significant improvement compared to the uncorrected case. Based on the established BNN framework, this study investigated the mass distributions of IND for ^{232}Th at incident neutron energies of 1 MeV and 13 MeV, and further explored the energy dependence of CUM for the selected nuclides.

The remainder of this paper is organized as follows. Section 2 introduces the theoretical framework of the BNN method. Section 3 provides detailed descriptions of the network construction and analysis of results, with Sect. 3.1 focusing on IND and Sect. 3.2 providing a comprehensive analysis of the CUM. Finally, Sect. 4 summarizes the key findings and methodological innovations of this study.

2 BNN model

A Bayesian neural network (BNN) is adopted in this study to predict fission product yields by combining Bayesian inference with the structure of traditional neural networks [65]. Unlike conventional neural networks, in which model parameters are fixed after training and produce a single deterministic output, BNN represents model parameters as probability distributions. This probabilistic formulation enables the BNN to provide both predictions and reliable estimates of the associated uncertainties.

The core of BNN lies in the posterior probability distribution of the model parameters,

$$p(\theta|x,t) = \frac{p(x,t|\theta)p(\theta)}{\int p(x,t|\theta)p(\theta)\mathrm{d}\theta}, \tag{1}$$

where $p(x,t|\theta)$ is the likelihood function that describes the probability of the observed data given the model parameters θ, and $p(\theta)$ is the prior distribution that represents prior beliefs about these parameters. The integral in the denominator serves as a normalization constant to ensure that the posterior distribution is valid. The posterior and predictive distributions are obtained via Markov chain Monte Carlo (MCMC) sampling methods, including Metropolis, Hybrid

Monte Carlo, and Slice sampling, which enables rigorous uncertainty quantification of the network parameters. As the training data accumulate, the influence of the prior diminishes in favor of the likelihood.

The likelihood function $p(x,t|\theta)$ is given by

$$p(x,t|\theta) = \exp\left(-\chi^2/2\right). \tag{2}$$

The discrepancy between the target and predicted values is quantified by the χ^2 loss function,

$$\chi^2(\theta) = \sum_{i=1}^{N} \left(\frac{t_i - f(x_i,\theta)}{\Delta t_i} \right)^2, \tag{3}$$

where t_i is the target value, $f(x_i,\theta)$ is the network prediction for input x_i, and Δt_i is the associated experimental uncertainty or noise term [66]. Minimizing χ^2 during training corresponds to maximizing the likelihood. This choice of loss function is motivated by its statistical consistency with Gaussian measurement errors and its emphasis on accurately reproducing high-yield regions, such as the bimodal peaks in fission product distributions, which are of primary physical interest in this study.

In Bayesian neural networks, a feed-forward neural network is used,

$$f(x,\theta) = a + \sum_{j=1}^{H} b_j \tanh\left(c_j + \sum_{i=1}^{l} d_{ji} x_i \right), \tag{4}$$

where $x = (x_1, x_2, \ldots, x_l)$ is the input vector consisting of l characteristics, typically including the proton number (Z), neutron number (N), and mass number (A) of the fissioning nuclei and fission fragments, and the excitation energy (E) of the compound nucleus. $\theta = \{a, b_j, c_j, d_{ji}\}$ represents the values of the model parameters, where d_{ji} is the connection weight between the input layer and the hidden layer, indicating the influence of the input characteristics on the hidden neurons. c_j is the bias of the hidden layer, which determines the baseline level when there is no contribution from the input layer to the activation function. b_j is the connection weight between the hidden layer and the output layer, representing the contribution weight of each hidden neuron to the final output. a is the bias of the output layer. The nonlinear tanh activation function enables an accurate approximation of complex continuous functions. Figure 1 shows the schematic structure of the single-hidden-layer Bayesian neural network used for the fission yield evaluation.

Given a new input x_n, the network prediction is the expected value over the posterior,

$$\langle f(x_n,\theta)\rangle = \int f(x_n,\theta) p(\theta|x,t) \mathrm{d}\theta. \tag{5}$$

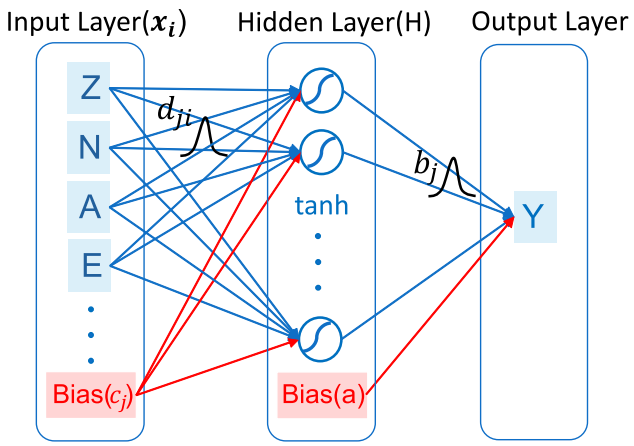

Fig. 1 (Color online) Schematic of the single-hidden-layer Bayesian neural network for fission yield evaluation. The input layer includes the proton and neutron numbers, mass numbers of fissioning nuclei and fission fragments, and excitation energy of the compound nucleus. The hidden layer contains H neurons with tanh activation function. The output layer provides the predicted fission yields. All connection weights (b_j, d_{ji}) and biases (a, c_j) are treated as probability distributions

Each prediction corresponding to a specific set of parameters is weighted by its posterior probability, and the integration yields the final predictive output of the BNN, which incorporates both the central estimate and uncertainty.

3 Results and discussion

3.1 Independent fission yield

Based on the fission yield dataset selected in this study, BNN models with both single and double hidden layers were constructed and evaluated. Comparative analysis revealed that the two-hidden-layer architecture provides better generalization performance and results in lower prediction errors than the single-hidden-layer. To further optimize the architecture and prevent overfitting from excessive complexity or underfitting from insufficient model capacity, the number of neurons per layer was systematically examined. For both simplicity and consistency, the same number of neurons was assigned to each of the two hidden layers of the network. This symmetric configuration not only ensures a balanced parameter distribution across the network but also reduces the number of hyperparameters to be tuned during model optimization. The neuron count varied from 16 to 40 in increments of four. Each configuration was trained under identical conditions using a fixed dataset and a hyperparameter set. During training, the total error in the training dataset was monitored across iterations to evaluate the convergence

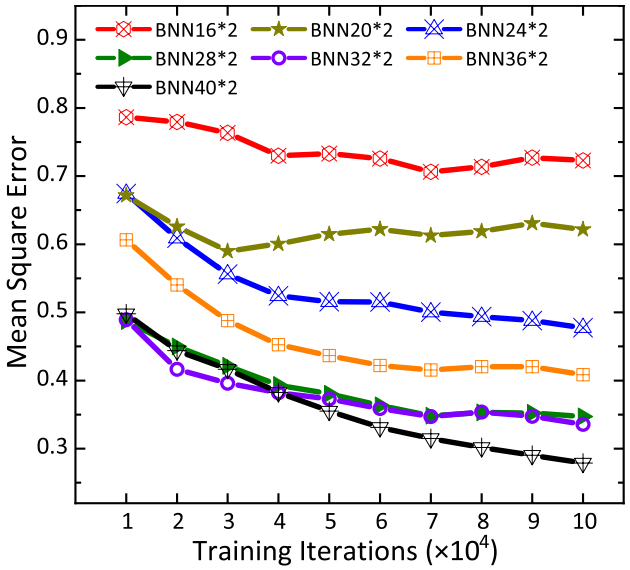

Fig. 2 (Color online) The variation in total training dataset error across different network architectures, as a function of training iterations. The selected networks are all two-hidden-layer networks, with the number of neurons in each layer starting from 16, increasing by 4 each time, up to a maximum of 40

behavior and prediction stability. The resulting error trends are shown in Fig. 2 provides a basis for selecting the optimal network configuration used in subsequent fission yield predictions.

Figure 2 illustrates the variation in the mean square error (MSE) during training for networks with different neuron counts per hidden layer. Under a fixed network architecture, the error gradually decreased with an increase in training iterations and stabilized as the number of iterations approached 10^5, indicating that convergence had been reached. Within the Bayesian neural network framework, we mitigate the risk of converging to local minima by employing a substantially large number of iterations, allowing the sampling process to thoroughly explore the parameter space. At a given number of training iterations, increasing the number of neurons per hidden layer leads to a noticeable reduction in the prediction error. However, this trend began to plateau when the neuron count reached 28, beyond which the additional reduction in error became marginal. This observation suggests that increasing the model complexity beyond this point does not lead to significant performance gains and may potentially introduce the risk of overfitting. To balance the predictive accuracy and model generalization, a configuration with two hidden layers and 28 neurons per layer was selected as the optimal network architecture.

In IND modeling, the mass distribution of fission product yields is of central importance. However, experimental data directly reporting the yield as a function of the mass number are limited. To address this issue and maximize the use of the available data, the training input was designed to include the neutron number of the fissioning nuclei, proton number, and mass number of the fission fragments, excitation energy of the compound nucleus, and corresponding IND of individual nuclides. The dataset used in IND includes 4,128 evaluated data points extracted from the JENDL database [11] and 112 experimental data points obtained from the EXFOR database [15]. The mass yield data from EXFOR were employed for validation. To further enhance the predictive performance of the BNN, additional physical constraints were added. Specifically, the odd–even effect is incorporated by assigning a value of +0.2 for even-proton-number fragments and −0.2 for odd-proton-number fragments, following the methodology described in Ref. [67]. In addition, isospin symmetry is accounted for by including the third component of isospin, defined as $(Z-N)/2$, as an input feature of the model. Once the BNN predicts the yields of individual nuclides, the mass yield distribution is reconstructed by summing the predicted yields of nuclides with the same mass numbers. This enables the generation of independent fission product mass distributions induced by incident neutrons on thorium isotopes, even when direct experimental data on mass yields are not available.

In Fig. 3, BNN_0 denotes the baseline model without additional physical constraints; $BNN_{1\text{-}1}$ incorporates the odd–even effect; $BNN_{1\text{-}2}$ includes isospin; and BNN_2 incorporates both constraints simultaneously by introducing the two corresponding input columns (odd–even and isospin) into the network. In Fig. 3a, corresponding to thermal neutron-induced fission of ^{227}Th, $BNN_{1\text{-}1}$ reduces the unphysical negative values present in BNN_0 but introduces an abnormal upturn near mass number 170. Similarly, $BNN_{1\text{-}2}$ suppresses the negative values and upturn but fails to reproduce the fine structure in the light fragment region. In contrast, BNN_2 not only eliminates these unphysical features but also retains the peak structure originally predicted by BNN_0, indicating that the simultaneous inclusion of both constraints results in a more precise representation of the fission mechanism and improves the model predictive accuracy. In Fig. 3b, for thermal neutron-induced fission of ^{229}Th, $BNN_{1\text{-}1}$ and $BNN_{1\text{-}2}$ exhibit similar behaviors as in Fig. 3a, whereas BNN_2 successfully reproduces the peak structure of the heavy fragment for the first time, which aligns well with the evaluated data. This suggests that the formation of heavy fission fragments is significantly influenced by the combined effects of the odd–even pattern and isospin. These results underscore the necessity of jointly incorporating both constraints to advance the theoretical modeling of the production of heavy fission fragments. In Fig. 3c, which shows neutron-induced fission of ^{232}Th at 0.5 MeV, BNN_0 exhibits an abnormal upturn around mass number 70 and significantly underestimates the yields in the 138–144 mass range relative to the evaluated data. $BNN_{1\text{-}1}$ corrects the heavy fragment

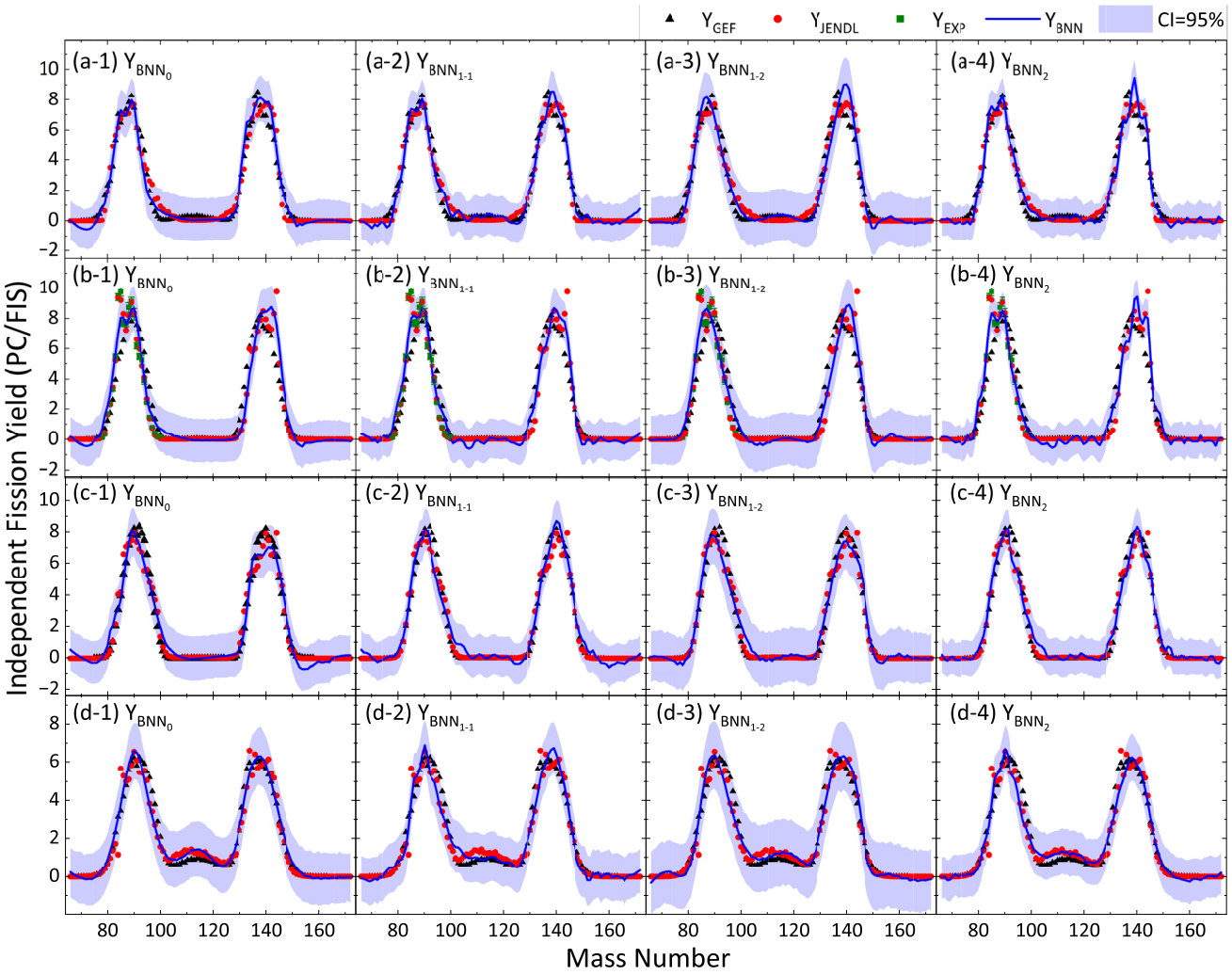

Fig. 3 (Color online) Comparison of independent fission product yield distributions as a function of mass number for thorium isotopes induced by neutrons of different energies, based on various data sources and BNN model predictions. Panels **a-1** to **a-4** show the mass yield distributions for the thermal neutron-induced fission of ^{227}Th. Panels **b-1** to **b-4** correspond to the thermal neutron-induced fission of ^{229}Th. Panels **c-1** to **c-4** correspond to the fission of ^{232}Th induced by 0.5 MeV neutrons, and panels **d-1** to **d-4** correspond to the fission of ^{232}Th induced by 14 MeV neutrons. BNN_0 denotes the predictions that do not incorporate additional physical constraints. $BNN_{1\text{-}1}$ includes an odd–even effect in the training data. $BNN_{1\text{-}2}$ incorporates isospin dependence, while BNN_2 includes both the odd–even effect and isospin dependence

underestimation, whereas $BNN_{1\text{-}2}$ mitigates the abnormal upturn and reduces negative yields. However, only BNN_2 resolves all these deficiencies simultaneously, demonstrating the best overall performance in reproducing the fission fragment mass yield distribution. In Fig. 3d, corresponding to 14 MeV neutron-induced fission of ^{232}Th, BNN_2 provides the most accurate description of the symmetric fission region and matches the evaluated data well in the light fragment region (mass 80–100), outperforming the other models in both respects. Across all four reaction systems, compared to BNN_0, $BNN_{1\text{-}1}$ results in a slightly narrower confidence band, whereas $BNN_{1\text{-}2}$ shows a modest increase in uncertainty. In contrast, BNN_2 yields a substantial reduction in the confidence band width, indicating significantly improved predictive reliability. This reduction in uncertainty further suggests that the combination of both physical constraints enhances model generalizability. In summary, while the odd–even effect and isospin each contribute to improving the BNN model performance, they have individual limitations. Their simultaneous incorporation into BNN_2 lead to the most substantial improvement in both yield prediction accuracy and uncertainty reduction, closely aligning with the evaluated data and demonstrating the robustness of the combined-constraint model. Despite the incorporation of additional physical constraints, Y_{BNN} still exhibited unphysical negative values. Reference [60] demonstrated

that applying a penalty on negative values improves both the representation of yield peak structures and the overall predictive accuracy. This penalty mechanism will be considered in future network design.

Figure 4 shows the predicted fission fragment mass distributions for ^{232}Th induced by 1 MeV and 13 MeV neutrons, with both energy points excluded from the training data. Y_{BNN_2} are compared with Y_{BNN_0} and the Y_{GEF} [17]. In Fig. 4a, BNN_2 eliminates the unphysical negative yields observed in BNN_0 around mass numbers $A = 150–160$. Moreover, in the mass range $A = 90–100$, Y_{BNN_2} shows an improved agreement with Y_{GEF}. In Fig. 4b, Y_{BNN_2} also suppresses the negative values in the mass range $A = 100–120$ and produces significantly closer to Y_{GEF} in the $A = 120–140$ region. In both panels, the confidence intervals (confidence intervals) of Y_{BNN_2} are noticeably narrower than those of Y_{BNN_0}, indicating reduced predictive uncertainty and improved generalization performance. These results suggest that the simultaneous inclusion of the odd–even effect and isospin enhances the physical realism of the model and underscores the importance of incorporating both effects in fission yield modeling.

3.2 Cumulative fission yield

The training dataset includes both the proton and neutron numbers of the fissioning nuclei and fission fragments, excitation energy of the compound nucleus, and cumulative fission yields. It comprises 4128 evaluated data points from the JENDL database [11] and 1258 experimental data points from the EXFOR database [15]. Based on the collected cumulative fission yield data, various BNN architectures, including single-hidden-layer and two-hidden-layer networks with varying numbers of neurons per layer, were systematically evaluated. Optimal performance was achieved using a two-hidden-layer architecture with 20 neurons per layer, which was adopted as the baseline model. Four configurations were tested: (1) without additional physical constraints (BNN_0), (2) with only the odd–even effect ($BNN_{1\text{-}1}$), (3) with only the isospin effect ($BNN_{1\text{-}2}$), and (4) with both physical constraints simultaneously (BNN_2). The implementation of these physical constraints follows the same approach as that in IND [67]. Comparative analysis against the evaluated data shows that the BNN_2 model, which incorporates both effects, achieves the best predictive accuracy and generalization capability among all the models. Consequently, only the BNN_2 model was retained for the subsequent analysis.

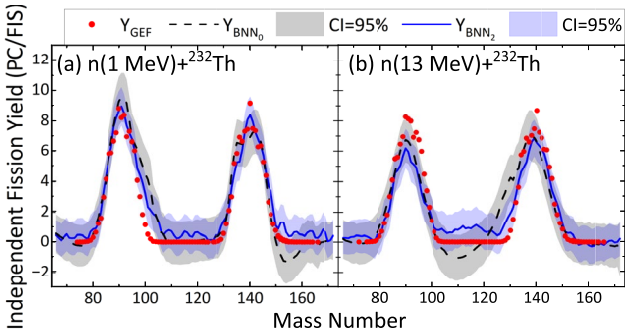

Fig. 4 (Color online) Mass distributions of independent fission yields from ^{232}Th induced by 1 MeV (**a**) and 13 MeV (**b**) neutrons. The results from BNN_0 without additional physical constraints, and BNN_2 including the odd–even effect and isospin, were compared with the independent yield data from GEF. Shaded bands represent 95% confidence intervals for the BNN predictions

Figure 5 compares the evaluated cumulative fission yields (Y_{JENDL}) with the predictions of the BNN without additional physical constraints (Y_{BNN_0}) and the physically constrained model (Y_{BNN_2}) for four representative reactions. In the thermal neutron-induced fission of thorium isotopes (Fig. 5a and b), the Y_{BNN_0} exhibits a systematic overestimation compared to Y_{JENDL}, particularly in low-yield (blue) regions, and fails to reproduce the characteristic yield peaks. In contrast, BNN_2 provides a much improved prediction, especially for light fragments, where Y_{BNN_2} closely matches Y_{JENDL}. In particular, two pronounced peaks (red spots) corresponding to ^{137}Ba and ^{140}Ce appear in both Y_{BNN_2} and Y_{JENDL}, demonstrating the model's ability to capture the key heavy fragment yields. In Fig. 5c, corresponding to a different actinide target, BNN_0 again overpredicts the yields in the low-value regions. This trend of overestimation was significantly mitigated in BNN_2, which was in better agreement with the evaluated distribution. Figure 5d, corresponding to fission at 14 MeV incident neutron energy, shows that BNN_2 substantially improves the yield predictions in the symmetric fission region, aligning more closely with Y_{JENDL} than BNN_0. In general, across the four reactions, Y_{BNN_2} demonstrated significantly better agreement with Y_{JENDL} than with Y_{BNN_0}, particularly in reproducing the heavy fragment yield peaks. These results demonstrate that incorporating the odd–even effect and isospin enhances the physical reliability and the predictive precision of the model. The mean squared error was reduced from 0.565 to 0.364, further confirming the effectiveness of the added physical constraints.

Figure 6 presents the cumulative fission yields for heavy fragments with mass numbers $A = 134 - 144$ from four neutron-induced Th fission reactions at different neutron energies. As fission products reach stability primarily through β-decay, these chain yields reflect the population of the final stable or long-lived nuclides along the decay chains. The evaluated data (Y_{JENDL}) show a clear odd–even staggering, with yields at odd mass numbers being notably higher than those of neighboring even-A isotopes. In addition, a pronounced enhancement was observed at $A = 140$, corresponding to the production of ^{140}Ce, which is a β-stable

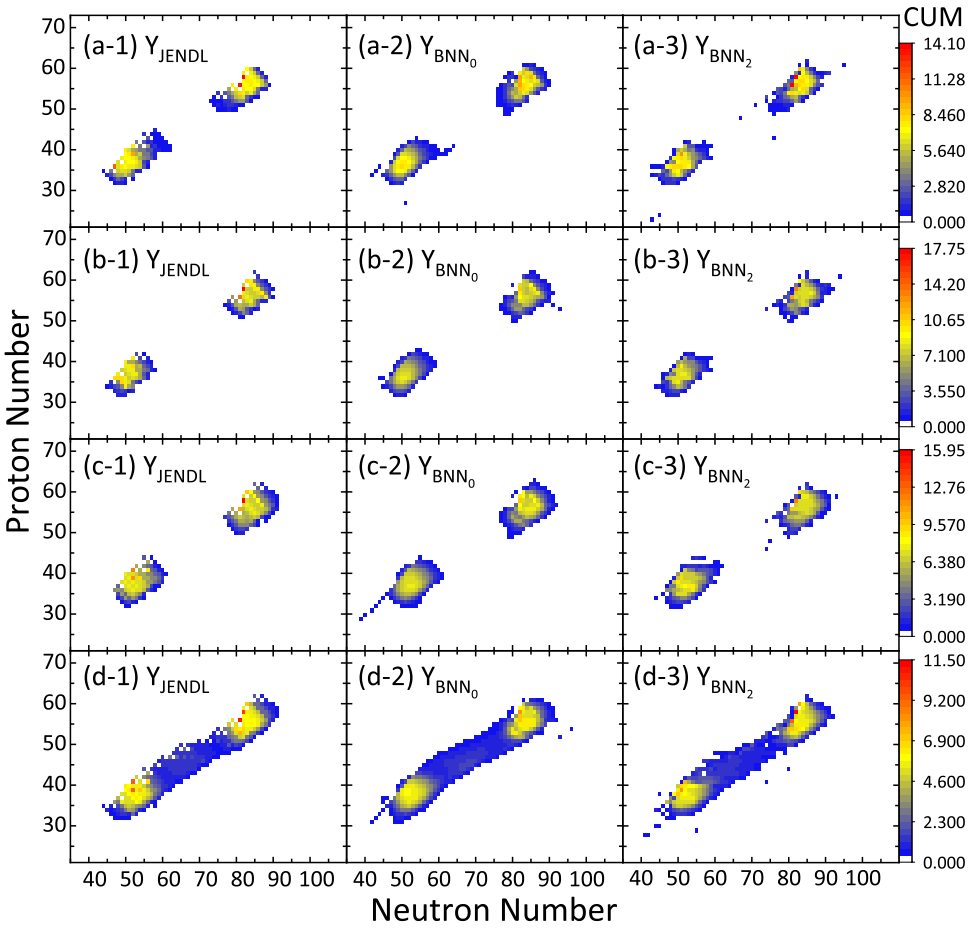

Fig. 5 (Color online) Comparisons of CUM distributions for thorium isotopes induced by neutrons at different incident energies. Shown are results from JENDL evaluated data (Y_{JENDL}), BNN predictions without additional physical constraints ($Y_{\mathrm{BNN_0}}$), and BNN predictions including odd–even effect and isospin ($Y_{\mathrm{BNN_2}}$). Panels **a** correspond to thermal neutron-induced fission of ^{227}Th, **b** to thermal neutron-induced fission of ^{229}Th, **c** to 0.5 MeV neutron-induced fission of ^{232}Th, and **d** to 14 MeV neutron-induced fission of ^{232}Th

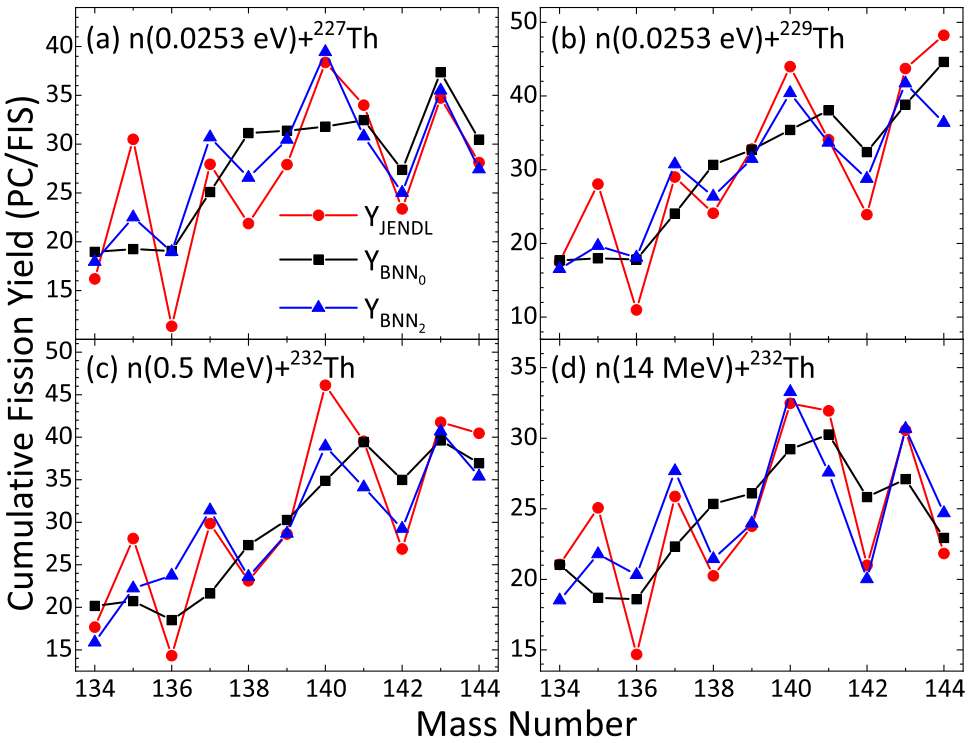

Fig. 6 (Color online) Comparisons of chain yields for fission products with mass numbers from 134 to 144. The evaluated results from JENDL (Y_{JENDL}), BNN predictions without additional physical constraints ($Y_{\mathrm{BNN_0}}$), and predictions including the odd–even effect and isospin ($Y_{\mathrm{BNN_2}}$) are shown. Panels **a** and **b** correspond to thermal neutron-induced fission of ^{227}Th and ^{229}Th, respectively, while **c** and **d** correspond to 0.5 MeV and 14 MeV neutron-induced fission of ^{232}Th

nuclide with a magic neutron number ($N = 82$) and one of the yield peaks identified in Fig. 5. BNN predictions without physical constraints (Y_{BNN_0}) show a smoother trend, failing to capture the odd–even structure and underestimating the peak at $A = 140$. In contrast, the constrained model (BNN_2), which incorporates both the odd–even effect and isospin, reproduces the evaluated pattern well (including the odd–even staggering and sharp rise at $A = 140$). These results demonstrate that integrating physical features into the BNN framework significantly improves its ability to capture decay chain effects and local nuclear structure signatures. Thus, the BNN_2 model offers a more accurate and physically interpretable prediction of the cumulative yields of fission products.

As shown in Fig. 6, the BNN_2 model more accurately captures the mass-dependent features of the fission product yields, particularly the odd–even staggering and the notable deviation around $A = 140$. To quantitatively assess the improvement from the incorporation of physical constraints, Figure 7 compares the ratios of the model predictions to the JENDL evaluations of the four neutron-induced fission reactions in thorium isotopes. The results show that the yield ratios predicted by BNN_2 (Y_{BNN_2}/Y_{JENDL}) are consistently closer to unity than those predicted by the original BNN_0 model (Y_{BNN_0}/Y_{JENDL}), indicating a significant enhancement in the prediction accuracy. This improvement was particularly evident for several mass numbers. For instance, at $A = 137$, the Y_{BNN_2} consistently aligns more closely with the Y_{JENDL} in all four cases, corresponding to the enhanced production of ^{137}Ba observed in Fig. 5. Around $A = 140$, the Y_{BNN_2} are nearly identical to the Y_{JENDL} in Fig. 7a and d, and also exhibit notable improvements over the Y_{BNN_0} in Fig. 7b and c, respectively. However, at $A = 136$, both Y_{BNN_0} and Y_{BNN_2} show notable deviations from Y_{JENDL}, suggesting that additional physical effects may influence the yields in this region and warrant further investigation. In summary, the overall trend of Y_{BNN_2}/Y_{JENDL} being consistently closer to unity than Y_{BNN_0}/Y_{JENDL} clearly demonstrates the benefit of incorporating the odd–even effect and isospin into the BNN framework. These physical enhancements significantly improved the model's ability to reproduce the evaluated cumulative fission yields for thorium-induced reactions, emphasizing their indispensable role in refining fission yield predictions.

Figure 8 presents the cumulative fission yields of four representative fission products—^{95}Zr, ^{99}Mo, ^{132}Te, and ^{131}I as a function of the incident neutron energy from 0 to 14 MeV. These nuclides were selected because of their significance in nuclear applications, environmental safety, and human health. Specifically, ^{95}Zr is a precursor of ^{95}Nb, which is a widely used redox indicator in reactor monitoring. ^{99}Mo, with a high decay branching ratio (88%) to ^{99m}Tc, plays a critical role in nuclear medicine. ^{132}Te promotes corrosion, shortening the service life of

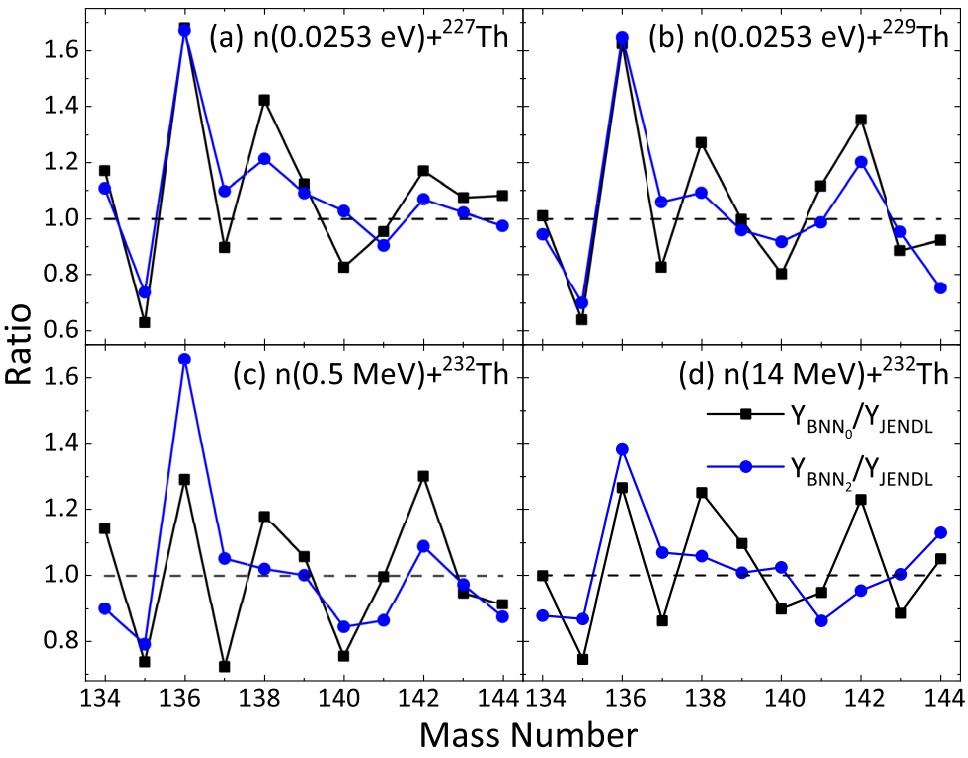

Fig. 7 (Color online) The yield ratios of fission products with mass numbers from 134 to 144, induced by neutrons of different energies, for thorium isotopes. The black squares represent the ratios of the initial BNN predictions without additional physical constraints (Y_{BNN_0}) to the evaluated data (Y_{JENDL}). The blue circles represent the ratios of BNN predictions incorporating the odd–even effect and isospin (Y_{BNN_2}) to the evaluated data (Y_{JENDL})

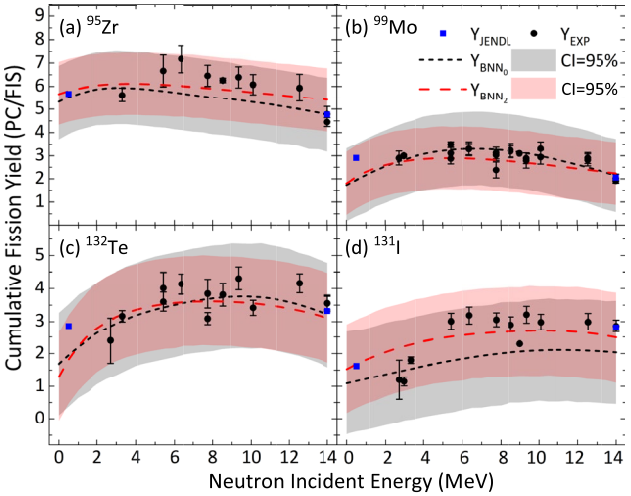

Fig. 8 (Color online) Cumulative fission yields of ^{95}Zr, ^{99}Mo, ^{132}Te, and ^{131}I as a function of incident neutron energy from 0 to 14 MeV. The experimental data are shown as black dots with error bars, while the blue squares denote the evaluated yields from the JENDL. The dashed black lines represent BNN predictions without additional physical constraints (Y_{BNN_0}), and the dashed red lines show the results incorporating the odd–even effect and isospin dependence (Y_{BNN_2}). Shaded areas correspond to the 95% confidence intervals for each prediction

structural materials, whereas ^{131}I is a radiotoxic nuclide with substantial biological impact. For ^{95}Zr (Fig. 8a), the yield initially increases, then gradually decreases at higher neutron energies (4–14 MeV). The BNN_0 model consistently underestimates the experimental data, whereas BNN_2 offers more accurate predictions across the energy range, with only a slight overestimation at 14 MeV. In the case of ^{99}Mo (Fig. 8b), the yield remains nearly constant from 2 to 12 MeV, with a small drop at 14 MeV. The BNN_2 predictions accurately captured this behavior and corrected the underestimation observed in BNN_0 at thermal energy (0.0253 eV). For ^{132}Te (Fig. 8c), the yield shows a pronounced increase at low energies, followed by a gradual decline beyond 8 MeV. The BNN_2 model matches the experimental trends more closely than BNN_0, particularly in the 0–4 MeV region. As shown in Fig. 8d, the yield of ^{131}I rises with increasing neutron energy. The predictions of BNN_2 align well with the experimental and evaluated data above 5 MeV and at thermal energy; however, both BNN predictions slightly overestimate the experimental results between 2 and 4 MeV. Overall, all experimental points fell within the 95% confidence intervals of the BNN predictions. Notably, the confidence bands associated with BNN_2 are narrower than those of BNN_0, demonstrating that incorporating odd–even effects and isospin corrections not only improves the predictive accuracy but also reduces the model uncertainty.

4 Summary

In this study, a Bayesian neural network (BNN) was employed to evaluate both independent (IND) and cumulative fission product yields (CUM), with the goal of improving the predictive accuracy beyond the limitations posed by sparse and inconsistent experimental data available only at a few neutron energies (thermal, 0.5 MeV, and 14 MeV). In the evaluation of IND, the input features were optimized by incorporating the proton and mass numbers of the fission fragments, along with their corresponding yields. This enabled the use of a broader set of experimental data for model training. A two-hidden-layer architecture with 28 neurons per layer was adopted based on the error minimization analysis. The incorporation of the odd–even effect and isospin significantly enhanced the predictive performance of the model. When both physical constraints were applied simultaneously, the model effectively suppressed unphysical negative yields, mitigated abnormal upturns, and reproduced the fine structures in the heavy fragment region. The uncertainty of the prediction, as reflected in the 95% confidence intervals, was also substantially reduced. For CUM evaluation, a two-hidden-layer architecture with 20 neurons per layer was selected after comprehensive testing of various configurations, including single-hidden-layer and two-hidden-layer networks with different neuron counts. Comparative studies were performed, including single-nuclide yield comparisons, analysis of odd–even staggering in mass yields (particularly in the A =134–144 region), and yield ratio Y_{BNN}/Y_{JENDL} analysis. These results demonstrate that the simultaneous incorporation of odd–even effects and isospin constraints significantly improved the reliability of the yield predictions. The model more accurately captured the features of stable nuclide production and successfully reproduced the anomalous structure near $A = 140$. Overall, our study demonstrates that combining physical constraints, particularly the odd–even effect and isospin, significantly enhances the performance and robustness of BNN-based fission yield evaluations. These findings suggest that such physical features should be systematically incorporated into future data-driven models and theoretical approaches to improve the accuracy of fission yield predictions.

Author Contributions Chun-Wang Ma and Chun-Yuan Qiao contributed to the study conception and design. Material preparation, data collection, and analysis were performed by Chun-Yuan Qiao and Ya-Xuan Wang. The first draft of the manuscript was written by Chun-Yuan Qiao and Ya-Xuan Wang. All authors commented on previous versions of the manuscript and read and approved the final version.

Data Availability The data that support the findings of this study are openly available in Science Data Bank at https://cstr.cn/31253.11.sciencedb.j00186.00865 and https://www.doi.org/10.57760/sciencedb.j00186.00865.

Declarations

Conflict of interest Chun-Wang Ma and Jun-Chen Pei are editorial board members for Nuclear Science and Techniques and were not involved in the editorial review, or the decision to publish this article. All authors declare that there are no conflict of interest.

References

1. J.H. Hamilton, S. Hofmann, Y. Oganessian, Search for superheavy nuclei. Annu. Rev. Nucl. Part. Sci. **63**, 383–405 (2013). https://doi.org/10.1146/annurev-nucl-102912-144535
2. J.C. Pei, W. Nazarewicz, J.A. Sheikh et al., Fission barriers of compound superheavy nuclei. Phys. Rev. Lett. **102**, 192501 (2009). https://doi.org/10.1103/PhysRevLett.102.192501
3. G. Mention, M. Fechner, T. Lasserre et al., Reactor antineutrino anomaly. Phys. Rev. D **83**, 073006 (2011). https://doi.org/10.1103/PhysRevD.83.073006
4. A.A. Sonzogni, E.A. McCutchan, T.D. Johnson et al., Effects of fission yield data in the calculation of antineutrino spectra for ^{235}U(n, fission) at thermal and fast neutron energies. Phys. Rev. Lett. **116**, 132502 (2016). https://doi.org/10.1103/PhysRevLett.116.132502
5. T.A. Mueller, D. Lhuillier, M. Fallot et al., Improved predictions of reactor antineutrino spectra. Phys. Rev. C **83**, 054615 (2011). https://doi.org/10.1103/PhysRevC.83.054615
6. S. Goriely, J.L. Sida, J.F. Lemaître et al., New fission fragment distributions and r-process origin of the rare-earth elements. Phys. Rev. Lett. **111**, 242502 (2013). https://doi.org/10.1103/PhysRevLett.111.242502
7. M. Eichler, A. Arcones, A. Kelic et al., The role of fission in neutron star mergers and its impact on the r-process peaks. Astrophys. J. **808**, 30 (2015). https://doi.org/10.1088/0004-637X/808/1/30
8. J. Sadhukhan, S.A. Giuliani, Z. Matheson et al., Efficient method for estimation of fission fragment yields of r-process nuclei. Phys. Rev. C **101**, 065803 (2020). https://doi.org/10.1103/PhysRevC.101.065803
9. M.H. Jiang, H.J. Xu, Z.M. Dai, Advanced fission energy program-TMSR nuclear energy system. Bull. Chin. Acad. Sci. **27**, 366–374 (2012). https://doi.org/10.3969/j.issn.1000-3045.2012.03.016
10. X.Z. Cai, Z.M. Dai, H.J. Xu, Thorium molten salt reactor nuclear energy system. Physics **45**, 578–590 (2016). https://doi.org/10.7693/wl20160904
11. Japanese evaluated nuclear data library (jendl), https://www.jendl.org/
12. M. Chadwick, M. Herman, P. Obložinský et al., ENDF/B-VII.1 Nuclear data for science and technology: cross sections, covariances, fission product yields and decay data. Nucl. Data Sheets **112**, 2887–2996 (2011). https://doi.org/10.1016/j.nds.2011.11.002
13. Z.G. Ge, Z.X. Zhao, H.H. Xia et al., The updated version of Chinese evaluated nuclear data library (CENDL-3.1). J. Korean Phys. Soc. **59**, 1052–1056 (2011). https://doi.org/10.3938/jkps.59.1052
14. A.J.M. Plompen, O. Cabellos, C. De Saint Jean et al., The joint evaluated fission and fusion nuclear data library, JEFF-3.3. Eur. Phys. J. A **56**, 181 (2020). https://doi.org/10.1140/epja/s10050-020-00141-9
15. Experimental nuclear reaction data(EXFOR), https://www-nds.iaea.org/exfor/
16. U. Brosa, S. Grossmann, A. Müller, Nuclear scission. Phys. Rep. **197**, 167–262 (1990). https://doi.org/10.1016/0370-1573(90)90114-H
17. K.H. Schmidt, B. Jurado, C. Amouroux et al., General description of fission observables: GEF model code. Nucl. Data Sheets **131**, 107–221 (2016). https://doi.org/10.1016/j.nds.2015.12.009
18. H.F. Zhang, L.H. Wang, J.P. Yin et al., Performance of the Levenberg-Marquardt neural network approach in nuclear mass prediction. J. Phys. G Nucl. Part. Phys. **44**, 045110 (2017). https://doi.org/10.1088/1361-6471/aa5d78
19. A. Boehnlein, M. Diefenthaler, N. Sato et al., Colloquium: machine learning in nuclear physics. Rev. Mod. Phys. **94**, 031003 (2022). https://doi.org/10.1103/RevModPhys.94.031003
20. P. Vicente-Valdez, L. Bernstein, M. Fratoni, Nuclear data evaluation augmented by machine learning. Ann. Nucl. Energy **163**, 108596 (2021). https://doi.org/10.1016/j.anucene.2021.108596
21. Z.M. Niu, H.Z. Liang, Nuclear mass predictions based on Bayesian neural network approach with pairing and shell effects. Phys. Lett. B **778**, 48–53 (2018). https://doi.org/10.1016/j.physletb.2018.01.002
22. Z.X. Yang, X.H. Fan, P. Yin et al., Taming nucleon density distributions with deep neural network. Phys. Lett. B **823**, 136650 (2021). https://doi.org/10.1016/j.physletb.2021.136650
23. X.H. Wu, P.W. Zhao, Predicting nuclear masses with the kernel ridge regression. Phys. Rev. C **101**, 051301 (2020). https://doi.org/10.1103/PhysRevC.101.051301
24. X.C. Ming, H.F. Zhang, R.R. Xu et al., Nuclear mass based on the multi-task learning neural network method. Nucl. Sci. Tech. **33**, 48 (2022). https://doi.org/10.1007/s41365-022-01031-z
25. R. Utama, J. Piekarewicz, H.B. Prosper, Nuclear mass predictions for the crustal composition of neutron stars: a Bayesian neural network approach. Phys. Rev. C **93**, 014311 (2016). https://doi.org/10.1103/PhysRevC.93.014311
26. R. Utama, J. Piekarewicz, Refining mass formulas for astrophysical applications: a Bayesian neural network approach. Phys. Rev. C **96**, 044308 (2017). https://doi.org/10.1103/PhysRevC.96.044308
27. Z.M. Niu, H.Z. Liang, Nuclear mass predictions with machine learning reaching the accuracy required by r-process studies. Phys. Rev. C **106**, L021303 (2022). https://doi.org/10.1103/PhysRevC.106.L021303
28. Z.M. Niu, J.Y. Fang, Y.F. Niu, Comparative study of radial basis function and Bayesian neural network approaches in nuclear mass predictions. Phys. Rev. C **100**, 054311 (2019). https://doi.org/10.1103/PhysRevC.100.054311
29. Y.F. Liu, C. Su, J. Liu et al., Improved Naive Bayesian probability classifier in predictions of nuclear mass. Phys. Rev. C **104**, 014315 (2021). https://doi.org/10.1103/PhysRevC.104.014315
30. D. Wu, C.L. Bai, H. Sagawa et al., Calculation of nuclear charge radii with a trained feed-forward neural network. Phys. Rev. C **102**, 054323 (2020). https://doi.org/10.1103/PhysRevC.102.054323
31. S. Akkoyun, T. Bayram, S.O. Kara et al., An artificial neural network application on nuclear charge radii. J. Phys. G Nucl. Part. Phys. **40**, 055106 (2013). https://doi.org/10.1088/0954-3899/40/5/055106
32. R. Utama, W.C. Chen, J. Piekarewicz, Nuclear charge radii: density functional theory meets Bayesian neural networks. J. Phys. G Nucl. Part. Phys. **43**, 114002 (2016). https://doi.org/10.1088/0954-3899/43/11/114002
33. Y.F. Ma, C. Su, J. Liu et al., Predictions of nuclear charge radii and physical interpretations based on the Naive Bayesian probability classifier. Phys. Rev. C **101**, 014304 (2020). https://doi.org/10.1103/PhysRevC.101.014304
34. Y.Y. Cao, J.Y. Guo, B. Zhou, Predictions of nuclear charge radii based on the convolutional neural network. Nucl. Sci. Tech. **34**, 152 (2023). https://doi.org/10.1007/s41365-023-01308-x

35. C.Q. Li, C.N. Tong, H.J. Du et al., Deep learning approach to nuclear masses and α-decay half-lives. Phys. Rev. C **105**, 064306 (2022). https://doi.org/10.1103/PhysRevC.105.064306
36. Z.M. Niu, H.Z. Liang, B.H. Sun et al., Predictions of nuclear β-decay half-lives with machine learning and their impact on r-process nucleosynthesis. Phys. Rev. C **99**, 064307 (2019). https://doi.org/10.1103/PhysRevC.99.064307
37. P. Li, Z.M. Niu, Y.F. Niu, Selection of abnormal trends in nuclear β-decay half-lives by neural network and exploration of the physical mechanisms. Nucl. Sci. Tech. **36**, 50 (2025). https://doi.org/10.1007/s41365-025-01663-x
38. D. Liu, A.N. A, Z.Z. Qin, et al., Neural network study of the nuclear ground-state spin distribution within a random interaction ensemble. Nucl. Sci. Tech. **35**(64), (2024). https://doi.org/10.1007/s41365-024-01424-2
39. Z.A. Wang, J.C. Pei, Y. Liu et al., Bayesian evaluation of incomplete fission yields. Phys. Rev. Lett. **123**, 122501 (2019). https://doi.org/10.1103/PhysRevLett.123.122501
40. A. Lovell, A. Mohan, P. Talou et al., Constraining fission yields using machine learning. EPJ Web Conf. **211**, 04006 (2019). https://doi.org/10.1051/epjconf/201921104006
41. Q.F. Song, L. Zhu, H. Guo et al., Verification of neutron-induced fission product yields evaluated by a tensor decomposition model in transport-burnup simulations. Nucl. Sci. Tech. **34**, 32 (2023). https://doi.org/10.1007/s41365-023-01176-5
42. Q.F. Song, L. Zhu, B.S. Cai et al., Image processing of isotope yield in neutron-induced fission. Phys. Rev. C **107**, 044609 (2023). https://doi.org/10.1103/PhysRevC.107.044609
43. L. Tong, R.N. He, S.W. Yan, Prediction of neutron-induced fission product yields by a straightforward k-nearest-neighbor algorithm. Phys. Rev. C **104**, 064617 (2021). https://doi.org/10.1103/PhysRevC.104.064617
44. D. Peng, H.L. Wei, X.X. Chen et al., Bayesian evaluation of residual production cross sections in proton-induced nuclear spallation reactions. J. Phys. G Nucl. Part. Phys. **49**, 085102 (2022). https://doi.org/10.1088/1361-6471/AC7069
45. D. Peng, H.L. Wei, J. Pu et al., Bayesian neural network prediction methods for fragment cross sections in proton-induced spallation reactions. Sci. Sin. Phys. Mech. Astron. **52**, 252012 (2022). https://doi.org/10.1360/SSPMA-2021-0298
46. C.W. Ma, D. Peng, H.L. Wei et al., A bayesian-neural-network prediction for fragment production in proton induced spallation reaction. Chin. Phys. C **44**, 124107 (2020). https://doi.org/10.1088/1674-1137/abb657
47. C.W. Ma, D. Peng, H.L. Wei et al., Isotopic cross-sections in proton induced spallation reactions based on the Bayesian neural network method. Chin. Phys. C **44**, 014104 (2020). https://doi.org/10.1088/1674-1137/44/1/014104
48. C.W. Ma, X.B. Wei, X.X. Chen et al., Precise machine learning models for fragment production in projectile fragmentation reactions using Bayesian neural networks. Chin. Phys. C **46**, 074104 (2022). https://doi.org/10.1088/1674-1137/ac5efb
49. C.W. Ma, X.X. Chen, X.B. Wei et al., Systematic behavior of fragments in Bayesian neural network models for projectile fragmentation reactions. Phys. Rev. C **108**, 044606 (2023). https://doi.org/10.1103/PhysRevC.108.044606
50. X.B. Wei, H.L. Wei, C.W. Ma et al., Predictions from several models for the cross sections of light neutron-rich isotopes by Q_g systematics in ^{40}Ar projectile-fragmentation reactions. Phys. Rev. C **111**, 034607 (2025). https://doi.org/10.1103/PhysRevC.111.034607
51. X.B. Wei, H.L. Wei, Y.T. Wang et al., Multiple-models predictions for drip line nuclides in projectile fragmentation of ^{40,48}Ca, ^{58,64} Ni, and ^{78,86} Kr at 140 MeV/u. Nucl. Sci. Tech. **33**, 155 (2022). https://doi.org/10.1007/s41365-022-01137-4
52. Y.Y. Li, F. Zhang, J. Su, Improvement of the Bayesian neural network to study the photoneutron yield cross sections. Nucl. Sci. Tech. **33**, 135 (2022). https://doi.org/10.1007/s41365-022-01131-w
53. Q.K. Sun, Y. Zhang, Z.R. Hao et al., Enhancing reliability in photonuclear cross-section fitting with Bayesian neural networks. Nucl. Sci. Tech. **36**, 52 (2025). https://doi.org/10.1007/s41365-024-01611-1
54. W.B. He, Q.F. Li, Y.G. Ma et al., Machine learning in nuclear physics at low and intermediate energies. Sci. China Phys. Mech. Astron. **66**, 282001 (2023). https://doi.org/10.1007/s11433-023-2116-0
55. C.Y. Qiao, J.C. Pei, Z.A. Wang et al., Study of energy dependence of neutron-induced fission yield of ^{235}U with Baysian machine learning. At. Energy Sci. Technol. (in Chinese) **56**, 937–943 (2022). https://doi.org/10.7538/yzk.2022.youxian.0198
56. D.R. Phillips, R.J. Furnstahl, U. Heinz et al., Get on the band wagon: a Bayesian framework for quantifying model uncertainties in nuclear dynamics. J. Phys. G Nucl. Part. Phys. **48**, 072001 (2021). https://doi.org/10.1088/1361-6471/abf1df
57. V. Kejzlar, L. Neufcourt, W. Nazarewicz et al., Statistical aspects of nuclear mass models. J. Phys. G Nucl. Part. Phys. **47**, 094001 (2020). https://doi.org/10.1088/1361-6471/ab907c
58. Z.A. Wang, J.C. Pei, Y.J. Chen et al., Bayesian approach to heterogeneous data fusion of imperfect fission yields for augmented evaluations. Phys. Rev. C **106**, L021304 (2022). https://doi.org/10.1103/PhysRevC.106.L021304
59. J.Y. Yi, C.Y. Qiao, J.C. Pei et al., Bayesian machine learning for the uncertainty evaluation of nuclear fission product yields. Sci. Sin. Phys. Mech. Astron. **52**, 123–129 (2022). https://doi.org/10.1360/SSPMA-2021-0340
60. Z.A. Wang, J.C. Pei, Optimizing multilayer Bayesian neural networks for evaluation of fission yields. Phys. Rev. C **104**, 064608 (2021). https://doi.org/10.1103/PhysRevC.104.064608
61. X.W. Jia, J. Willard, A. Karpatne et al., Physics-guided machine learning for scientific discovery: an application in simulating lake temperature profiles. ACM/IMS Trans. Data Sci. **2**(3), 20 (2021). https://doi.org/10.1145/3447814
62. G.E. Karniadakis, I.G. Kevrekidis, L. Lu et al., Physics-informed machine learning. Nat. Rev. Phys. **3**, 422–440 (2021). https://doi.org/10.1038/s42254-021-00314-5
63. D.R. Phillips, R.J. Furnstahl, U. Heinz et al., Get on the band wagon: a Bayesian framework for quantifying model uncertainties in nuclear dynamics. J. Phys. G Nucl. Part. Phys. **48**, 072001 (2021). https://doi.org/10.1088/1361-6471/abf1df
64. D. Neudecker, O. Cabellos, A.R. Clark et al., Informing nuclear physics via machine learning methods with differential and integral experiments. Phys. Rev. C **104**, 034611 (2021). https://doi.org/10.1103/PhysRevC.104.034611
65. R.M. Neal, Bayesian learning for neural networks. Springer, New York, (2012). https://doi.org/10.1007/978-1-4612-0745-0
66. L. Neufcourt, Y.C. Cao, W. Nazarewicz et al., Bayesian approach to model-based extrapolation of nuclear observables. Phys. Rev. C **98**, 034318 (2018). https://doi.org/10.1103/PhysRevC.98.034318
67. C.Y. Qiao, J.C. Pei, Z.A. Wang et al., Bayesian evaluation of charge yields of fission fragments of ^{239}U. Phys. Rev. C **103**, 034621 (2021). https://doi.org/10.1103/PhysRevC.103.034621